Cancer Nanotechnology

RESEARCH Open Access

Doxorubicin-loaded polymeric nanoparticles containing ketoester-based block and cholesterol moiety as specific vehicles to fight estrogen-dependent breast cancer

Paweł Misiak[1], Katarzyna Niemirowicz-Laskowska[2*], Karolina H. Markiewicz[1], Przemysław Wielgat[3], Izabela Kurowska[1,4], Robert Czarnomysy[5], Iwona Misztalewska-Turkowicz[1], Halina Car[2], Krzysztof Bielawski[5] and Agnieszka Z. Wilczewska[1*]

*Correspondence: katarzyna.niemirowicz@umb.edu.pl; agawilcz@uwb.edu.pl

[1] Faculty of Chemistry, University of Bialystok, Ciolkowskiego 1K, 15-245 Białystok, Poland
[2] Department of Experimental Pharmacology, Medical University of Bialystok, Mickiewicza 2A, 15-089 Białystok, Poland
[3] Department of Clinical Pharmacology, Medical University of Bialystok, Białystok, Poland
[4] Doctoral School of Exact and Natural Sciences, University of Bialystok, Białystok, Poland
[5] Department of Synthesis and Technology of Drugs, Medical University of Bialystok, Kilinskiego 1, 15-089 Białystok, Poland

Abstract

The presented research concerns the preparation of polymer nanoparticles (PNPs) for the delivery of doxorubicin. Several block and statistical copolymers, composed of ketoester derivative, *N*-isopropylacrylamide, and cholesterol, were synthesized. In the nanoprecipitation process, doxorubicin (DOX) molecules were kept in spatial polymeric systems. DOX-loaded PNPs show high efficacy against estrogen-dependent MCF-7 breast cancer cell lines despite low doses of DOX applied and good compatibility with normal cells. Research confirms the effect of PNPs on the degradation of the biological membrane, and the accumulation of reactive oxygen species (ROS), and the ability to cell cycle arrest are strictly linked to cell death.

Highlights

1. DDS based on cholesterol, ketoester, and NIPAAm, designed for the delivery of DOX.
2. The ketoester and arrangement of blocks are crucial for anticancer activity.
3. PNPs not only act as transporters but also sensitize the cell to DOX.
4. High cytotoxicity of DOX-loaded PNPs was achieved despite low doses of the drug.
5. PNPs have the proper size, shape, and ζ potential for efficient drug delivery.

Keywords: Polymeric nanoparticles, Cholesterol-end capped poly(*N*-isopropylacrylamide), Cell-penetrating molecules, Breast cancer, Doxorubicin, Smart drug delivery systems

Graphical Abstract

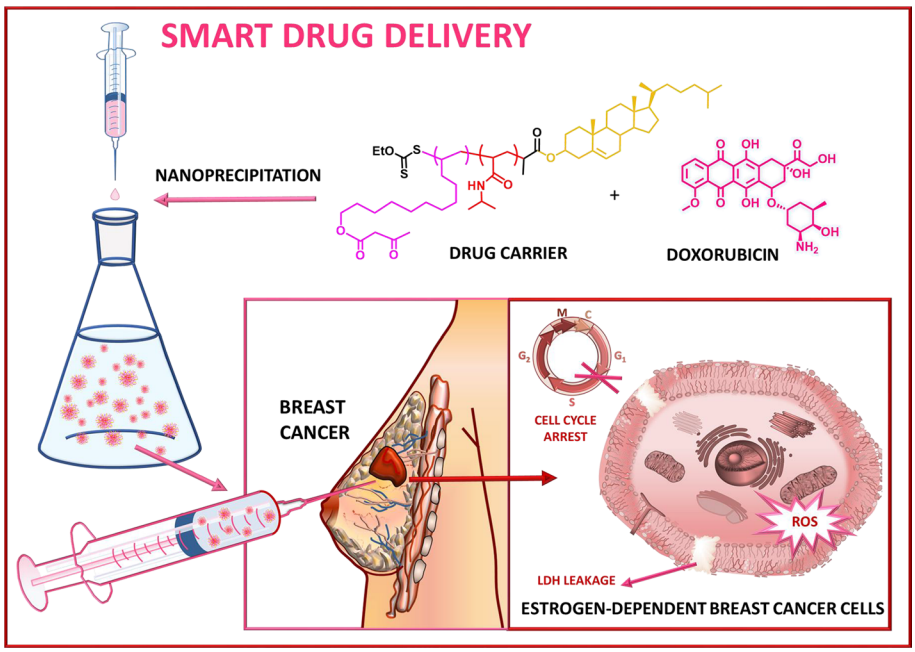

Introduction

In 2020, female breast cancer surpassed lung cancer and became the most commonly diagnosed cancer in the world and the leading cause of death in women (Sung et al. 2021). Every year for the past 3 years, the number of new cases has exceeded 2 million, and the number of deaths has exceeded 600,000 each year (d'Avanzo et al. 2021; Bray et al. 2018; Sung et al. 2021). A search for "breast cancer" in the Scopus database shows 558,676 results. The number of publications on this subject grows each year, with 33,597 documents in the past year alone. Despite great interest from the scientific community and the development of new therapeutic methods, the problem of breast cancer has not been solved. It should be emphasized that we are currently struggling with an increase in the expression of drug resistance mechanisms in cancer cells. Additional problems are associated with the pharmacokinetic parameters of drug stability in vivo. Moreover, achieving specific activity toward neoplastic cells also presents a huge challenge (Du et al. 2019; Wicki et al. 2015). The above-mentioned leads to numerous side effects that significantly hinder or prevent patients' ability to function normally.

Doxorubicin (DOX) is the most widely used drug in the treatment of breast cancer (Carvalho et al. 2009; Gonçalves et al. 2020). It is an organic compound from the anthracycline group. The anti-cancer effect is based on interaction with the DNA chain and inhibition of replication (Olim et al. 2021). This is due to the inhibition of topoisomerase II progression by stabilizing its complex with the DNA chain, which prevents further division and leads to cell death (Pommier et al. 2010; Tacar et al. 2012). This intercalation is confirmed by the crystal structures that show the flat aromatic part of DOX located between the two base pairs of DNA and the sugar part (six-membered daunosamine)

interacting with the surrounding base pairs (Frederick et al. 1990; Pigram et al. 1972). Unfortunately, doxorubicin as a non-specific drug causes several side effects in patients. The two most common phenomena leading to cytotoxicity are (I) inhibition of DNA replication in normal cells related to the DOX mechanism of action (Gonçalves et al. 2020; Hortobágyi 1997; Yang et al. 2014) and (II) cardiotoxicity (Safra 2003; Thigpen 2005; Volkova and Russell 2012). The latter requires the use of minimal doses. Historically, doses below 450 mg m^{-2} were considered safe (Rivankar 2014), and doses in the range of 450–550 mg m^{-2} resulted in congestive heart failure (CHF) in 5% of cases (Paul Launchbury and Habboubi 1993). Increasing the amount to 1000 mg m^{-2} led to an increase in the incidence to 50% of cases (Shan et al. 1996). Latter studies show that doxorubicin-induced CHF might occur at lower doses and at a greater frequency than previously noted (Hortobágyi 1997; Rivankar 2014).

Modern drug delivery systems (DDSs) are equipped with cell homing parts, one such molecule being cholesterol, the fundamental structural component of mammalian cell membranes. It is responsible for the integration, stiffness, and permeability of the membrane (Misiak et al. 2020a; Nes 2011; Sadava 2011). Cholesterol is also responsible for the structure of microdomains (lipid rafts). Additionally, it acts as a precursor in bile acids, sex hormones, and vitamin D biosynthesis (Cerqueira et al. 2016; Torchilin 2012). Polymeric carriers based on cholesterol are characterized by high biocompatibility and an affinity for cell membranes, which increases their uptake. This reduces the dose of drugs which, in turn, diminishes the risk of side effects (Avramović et al. 2020; Misiak et al. 2022; Olim et al. 2021; Zhang et al. 2016). In comparison with its free molecules, doxorubicin encapsulation into cholesterol-containing systems has a marked impact on the decreasing viability of breast cancer cells (Chen et al. 2019; Misiak et al. 2022; Olim et al. 2021; Yang et al. 2015; Zhang et al. 2014).

Poly(*N*-isopropylacrylamide) (PNIPAAm)-based systems are the most commonly used thermosensitive DOX carriers and are characterized by a lower critical solubility temperature (LCST) that is close to the physiological temperature (He et al. 2020; Misiak et al. 2020b). The phase transition temperature of PNIPAAms can be easily adjusted by adding different polymer blocks. A popular procedure to increase this temperature is the copolymerization of hydrophilic acrylic acid (Don et al. 2017). PNIPAAm-based vehicles showed excellent biocompatibility and enhanced therapeutic efficacy toward breast cancer cells compared to free-DOX (Misiak et al. 2022, Metawea et al. 2021, Shin et al. 2020.

These studies extend upon and demonstrate new aspects of our previous work (Misiak et al. 2020b), which concerned the physicochemical and biological properties of cholesterol end-capped poly(*N*-isopropylacrylamide)s of different molecular weights. This article presents three-partial copolymers consisting of cholesterol, NIPAAm, and an acetylacetone ester derivative. Each component plays an important role in influencing the effectiveness of the entire carrier, and the arrangement of the blocks is also important. The cholesterol moiety enables the penetrating of cell membranes. Thermosensitive and hydrophilic PNIPAAm is responsible for both the phase transition in the appropriate temperature range and the improvement of biocompatibility. The ketoester part provides the specificity of interaction with the studied breast cancer cells.

This work presents the synthesis and complete physicochemical characteristics of copolymers. Doxorubicin was introduced into polymer systems in the nanoprecipitation

process. Basic biological tests were carried out to assess the safety and cytotoxicity of the presented vehicles, i.e., hemocompatibility (hemolysis of red blood cells (RBC) and ability of immune cells to proliferate), the viability of cardiomyocyte cells, as well as anticancer potential against estrogen-dependent and estrogen-independent breast cancer cells. The mode of action of the carriers has been studied using spectrophotometric, luminometric, and flow cytometry-based assays. Results suggest that the studied systems are selective in the anticancer activity towards estrogen-dependent cancer cells.

Experimental

Materials and methods

Materials

The initiator, 2,2′-azobis(2-methylpropionitrile) (AIBN, MERCK) was recrystallized from chloroform. Monomer, *N*-isopropylacrylamide (NIPAAm, 99%, ACROS) was recrystallized from toluene-hexane (60:40, v/v), prior to use. Chain transfer agent (CTA, cholX (Dithiocarbonate derivative of cholesterol)) and cholesterol end-capped PNIPAAm (P1) were synthesized according to the previously published method (Misiak et al. 2020b). Methyl acetoacetate (AcacOMe, 99%, Aldrich), 1,10-Decanediol (pure, Fluka AG), acryloyl chloride ($\geq$ 97%, Aldrich), Triethylamine (Et_3N, Avantor), Phosphate Buffer Solution (PBS, pH = 7.4, GIBCO) and Dulbecco's Modified Eagle Medium (DMEM, GIBCO) were used as received. All organic solvents were purchased from Avantor Performance Materials, Poland S.A. and were distilled before use.

Methods

Nuclear magnetic resonance (NMR) The ^{1}H and ^{13}C NMR spectra were recorded on Bruker Avance II 400 or Avance DPX 200 spectrometers using $CDCl_3$ as a solvent.

Attenuated total reflectance Fourier transform infrared spectroscopy (ATR-FTIR) All ATR-FTIR spectra were recorded using the Thermo Scientific Nicolet 6700 FTIR spectrophotometer equipped with an ATR accessory. Spectra were ratioed against the background spectra and collected in the wavenumber range 4000 to 500 cm^{-1} by co-adding 32 scans with a resolution of 4 cm^{-1}.

Size exclusion chromatography (SEC) Molecular weights and molecular weight distributions of polymers were determined by size exclusion chromatography (SEC) using THF as an eluent at a flow rate of 1.0 mL min^{-1} at 35 °C. Before the analysis, polymers were carefully dissolved in the eluent (final concentration was 5 mg mL^{-1}) and filtered through a 0.45 μm PTFE filter. The samples were analyzed using a three-column set including KF-805, KF-804, and KF-802.5 (Shodex) and coupled with a three detector system: a refractometer thermostated at 35 °C (Optilab Rex, Wyatt technology), a UV detector (Prostar, Varian) set at 290 nm, and a multi-angle laser light scattering (MALS) detector (Mini Dawn, 3 angles, Wyatt technology). The dn/dc of **P1** (0.052 mL g^{-1}) was measured at 620 nm using a DNDC-2010 differential refractometer.

Fluorescence measurements A Hitachi F-7000 Fluorescence Spectrophotometer was used to determine critical micelle concentration (CMC) by the pyrene fluorescent probe

method adapted from the literature (Cammas et al. 1997; Wang et al. 2017, 2020). Ten microliters of pyrene stock solution (0.15 mM) were poured into empty vials, and acetone was evaporated by argon stream. Then, 3 mL of aqueous polymer solutions of various concentrations (10^{-4} to 2 mg mL^{-1}) were added to the vials and shaken vigorously. The mixtures were stored overnight in the refrigerator for equilibrium. Emission spectra (range 360–460 nm, excitation wavelength 339 nm, and slit width 2.5 nm) were recorded. The ratios between intensities of emission peaks at 373 and 393 nm (I_{373}/I_{393}) were plotted as a function of the polymer concentration. The CMC values were determined as the curve breakpoint. Fluorescence spectroscopy was also used to determine the quantity of encapsulated doxorubicin in polymer micelles. A calibration curve was fixed on DOX solutions in PBS with various concentrations (10^{-5} to 10^{-2} mg mL^{-1}). Emission spectra (range 460–700 nm, excitation wavelength 490 nm, and slit width 5 nm) were recorded. Emission band intensities were collected at a maximum fluorescence of around 550 nm. The linearity of the curve is in the concentration range from $2.5{\cdot}10^{-5}$ to 10^{-3} mg mL^{-1}. Synthesized polymeric micelles with encapsulated doxorubicin were dissolved in PBS to reach the concentration of 1 mg mL^{-1}. Then, fluorescence measurements were made under the same conditions as for the standard curve. The fluorescence band blue shift occurred because of the interaction with the polymer, so the intensities were read off at the maximum emission of about 540 nm.

Dynamic Light Scattering (DLS), Multiangle Dynamic Light Scattering (MADLS), and Electrophoretic Light Scattering (ELS) Dynamic Light Scattering (DLS) with either a horizontal or vertical polarizer or in a change of temperature, Multiangle Dynamic Light Scattering (MADLS), and Electrophoretic Light Scattering (ELS) were carried out using a Zetasizer Ultra (Malvern Panalytical Ltd., Malvern, UK) equipped with a 10 mW helium/neon laser ($l = 633$ nm) at 25 °C. The instrument settings were optimized automatically by employing the ZS XPLORER software (Malvern Panalytical Ltd., Malvern, UK). Polymeric nanoparticles were dissolved in PBS to reach a concentration of 0.5 mg mL^{-1} to study the colloidal stability of the aqueous solutions, the hydrodynamic diameter of obtained particles, and the aggregation temperature. All measurements were performed one week after dissolution. The particle sizes are expressed as the mean hydrodynamic diameter of 5 measurements. Zeta potential was measured in a High Concentration Zeta Potential Cell (Zen1010) due to the high conductivity of the solutions. The aggregation temperature (T_{agg}) was determined from the increase in the particle size value.

Turbidimetry The polymers were dissolved in deionized water to a concentration of 0.5 mg mL^{-1}. Then, the transmission spectra were recorded on a Jasco V-670 spectrophotometer in a wavelength range of 800–700 nm and a heating rate of 0.5 °C min^{-1}. The cloud points (T_{CP}) were determined from the transmission decrease at a wavelength of 750 nm.

Thermal analysis Thermogravimetric analyses (TGA) were performed on a Mettler Toledo Star TGA/DSC unit (Greifensee, Switzerland). A sample weighing 2–3 mg was placed in an aluminum oxide crucible and heated from 50 to 900 °C at 10 °C min^{-1} under an argon flow rate of 40 mL min^{-1}; an empty pan was used as the reference.

Differential scanning calorimetry (DSC) measurements were performed using a Mettler Toledo Star DSC unit (Greifensee, Switzerland). A sample (~ 2 mg) was placed in an aluminum crucible and: (1) heated from 0 to 200 °C at a rate of 20 °C min^{-1}, (2) held isothermally for 10 min, (3) cooled to − 20 °C at a rate − 20 °C min^{-1}, and, finally, (4) heated again to 480 °C at a rate of 10 °C min^{-1}. The measurements were performed under an argon flow rate of 200 mL min^{-1}, and an empty pan was used as the reference. The T_g was taken as the midpoint of the heat capacity change in the second heating run.

Transmission electron microscopy (TEM) For TEM imaging, polymers were prepared by lyophilization. First, 0.1 mg mL^{-1} aqueous solutions were prepared. Then, 3 μL of the sample was applied on a holey carbon copper grid (holey carbon-coated grids onto 300 mesh copper, SPI Supplies) and a surplus of the solution was removed with a tissue paper; the process was performed twice for more convenient and better imaging. After that, the grids were immersed in liquid nitrogen (LN_2) and lyophilized for 24 h. TEM images were taken using a Tecnai G2 X-Twin microscope. Images were captured at the accelerating voltage of 200 kV using cryotrap (copper trap equipped with LN_2 Dewar) as a cooling tool for the microscope column.

Lyophilization Samples were lyophilized on Christ Alpha 1–2 LDplus with double-chamber. Aqueous solutions of polymers were frozen with liquid nitrogen and then lyophilized for 24 h.

Biological studies

Hemocompatibility assessment The compatibility of tested PNPs with blood components was evaluated using a hemolysis assay. For this purpose, fresh human red blood cells (RBCs) obtained from healthy volunteers were used. The release of the hemoglobin from treated cells was examined. In the first step, the collected cells were suspended in phosphate-buffered saline (PBS) to establish a hematocrit of ~ 5%. Then, empty or DOX-loaded PNPs were added in the concentration range from 0.05 to 0.5 mg mL^{-1} and incubated for 1 h at 37 °C. Next, after centrifugation, the relative hemoglobin concentration in supernatants was spectrophotometrically measured at a wavelength of 540 nm. The 0% hemolysis was taken from samples after the addition of 10 μL PBS, while the 100% hemolysis was taken from samples in which 1% Triton X-100 was added to disrupt all cell membranes. The results are presented as hemolysis ratios.

The hemolytic activity of the tested polymeric nanoparticles was evaluated in blood samples from healthy adult volunteers under IRB approval: R-I-002/254/2019. This study was approved by the Institutional Review Board (IRB) of The Medical University of Bialystok. All subjects provided informed written consent, and the collected samples were anonymous.

Cell viability, proliferation, and metabolic activity The viability of breast cancer cells MCF-7 and MDA-MB-231, as well as cardiomyocyte H9C2(2-1) cells, were assessed using a Neutral Red test. In brief, the empty and DOX-loaded PNPs along with DOX in free form (0.5 μM), were added to cells at the concentrations of 0.05, 0.1, 0.25, and 0.5 mg mL^{-1} and incubated for 24 h at 37 °C. Then, the viability of cells was examined

using a spectrophotometric-based method—neutral red assay. After a 24 h incubation period, the neutral red solution (0.33%) was added to each well, and the mixture was incubated for 2 h. In the next step, the neutral red was removed, and the cells were carefully rinsed with Neutral Red Assay Fixative for 5–10 min. Then, after removing the fixative solution the incorporated dye was then solubilized in a solubilization solution (100 µL). Finally, the absorbance at a wavelength of 540 nm was measured and normalized to the control.

In the case of non-adherent cells, the metabolic activity of monocytic THP-1 cells was determined by the resazurin-based assay. After a 24 h exposure to PNPs (empty and DOX-loaded), as well as the DOX in free form (0.5 µM), 10 µL of resazurin was added to each well. The cells were incubated for 2–4 h in the dark at 37 °C with a 5% CO_2 atmosphere. The absorbance was measured at 570 nm (resazurin assay) using a Biotek microplate reader. The mean absorbance of the untreated cells served as the reference for calculating 100% cellular viability. The results were normalized to the control.

Mode of action

LDH release assay To assess the ability of tested PNPs to disrupt the plasma membrane of cancer cells, the detection of lactate dehydrogenase (LDH) release from treated MCF-7 was performed following a commercially available protocol. In brief, the addition of DOX (0.5 µM) and tested polymeric nanoparticles with or without DOX (0.5 mg mL^{-1}) was followed by a 24 h incubation period. Then, the medium (50 µL) was transferred into a 96 well plate mixed with 50 µL of Master Reaction. After 15 min of incubation, the absorbance was measured using a Biotek microplates reader at a wavelength of 450 nm.

ROS detection The assay was performed as directed by the manufacturer (ROS-Glo^{TM} H_2O_2 Assay). The DOX in free form (0.5 µM) and tested polymeric nanoparticles with or without DOX (0.5 mg mL^{-1}) were added to MCF-7 cells seeded on an opaque white 96 well plate. The H_2O_2 substrate solution was then added, bringing the final volume to 100 µL. The plate was incubated at 37 °C in a 5% CO_2 incubator for 6 h. After incubation, 100 µL of the ROS-Glo detection solution was added to each well. After an additional 20 min incubation at room temperature, luminescence was recorded using a Varioscan Lux (Thermo Scientific).

Cell cycle The effects of exposure of MCF-7 cells to the tested compounds on cell cycle progression were analyzed by flow cytometry. Cells were cultivated in 6 well plates and exposed both to DOX in free form (0.5 µM) and to tested polymeric nanoparticles with or without DOX (0.5 mg mL^{-1}) for 24 h. Before analysis, cells were washed with PBS and trypsinized with a 0.05% tripsin/0.02% EDTA solution. Cells were then collected and centrifuged (1500 rpm, 5 min, 4 °C), fixed with 70% ethanol, and stored at − 20 °C for at least 24 h. Then, cells were washed in PBS, centrifuged, treated with DNase-free RNase A Solution (Promega; 50 µg mL^{-1}), and stained with 100 µg mL^{-1} of propidium iodide. Analysis of cell cycle distribution was performed using the fluorescence image cytometer FACSCanto II flow cytometer (BD Biosciences Systems, USA).

Statistical analysis

Statistical analyses were performed using Statistica 13.3 software (StatSoft Inc., Tulsa, OK, USA). The data were analyzed using standard statistical analyses, including Student's t-Test (for independent samples), where p-values less than 0.05 were considered significant.

Synthetic procedures

Synthesis of 10-hydroxydecyl 3-oxobutanoate A 1,10-Decanediol (3486 g, 20 mmol, 2 eq.) was dropped into a solution of methyl acetoacetate (1.079 mL, 10 mmol, 1 eq.), triethylamine (1.812 mL, 13 mmol, 1.3 eq.) in toluene (100 mL). The mixture was stirred at 110 °C and after 6 h and 30 min was cooled to room temperature. The solution was decanted from the excess of the crystallized diol, which was washed several times with toluene. The toluene fractions were combined and evaporated on a rotary evaporator. The obtained product was purified by column chromatography (hexane: ethyl acetate, 8:2) to result in an yellowish liquid (2.47 g, 96%). **Ketoester form (95%): ^{1}H NMR (400 MHz, $CDCl_3$, δ, ppm):** 4.13 (t, 2H, H-3), 3.61 (t, 2H, H-7), 3.43 (s, 2H, H-2), 2.25 (s, 3H, H-1), 1.73 (s, 1H, H-8), 1.62 (m, 2H, H-4), 1.54 (m, 2H, H-6), 1.27 (m, 12H, H-5). **^{13}C NMR (100 MHz, $CDCl_3$, δ, ppm):** 200.6 (C=O), 167.2 (C=O), 65.5 (CH_2), 62.9 (CH_2), 50.0 (CH_2), 32.7 (CH_2), 30.1 (CH_3), 29.4 (2xCH_2), 29.3 (CH_2), 29.0 (CH_2), 28.4 (CH_2), 25.7 (CH_2), 25.6 (CH_2). **Enol form (5%): ^{1}H NMR (400 MHz, $CDCl_3$, δ, ppm):** 12.08 (s, 1H, H-9), 4.96 (s, 1H, H-10), 3.61 (t, 2H, H-7), 1.73 (s, 1H, H-8), 1.62 (m, 2H, H-4), 1.54 (m, 2H, H-6), 1.27 (m, 12H, H-5). **^{13}C NMR (100 MHz, $CDCl_3$, δ, ppm):** 175.3 (C–OH), 172.7 (CH), 65.5 (CH_2), 62.9 (CH_2), 50.0 (CH_2), 32.7 (CH_2), 30.1 (CH_3), 29.4 (2xCH_2), 29.3 (CH_2), 29.0 (CH_2), 28.4 (CH_2), 25.7 (CH_2), 25.6 (CH_2). **FT-IR (ATR, ν) cm^{-1}:** 3398, 3331, 2920, 2850, 1736, 1716, 1651, 1463, 1360, 1331, 1279, 1271, 1237, 1154, 1058, 1049, 1018, 970, 803, 728, 667, 613.

Synthesis of 10-(acryloyloxy)decyl-3-oxobutanoate (AcacP) A 250 mL round bottom flask was charged with 10-hydroxydecyl-3-oxobutanoate (1 g, 3.87 mmol, 1 eq), triethylamine (0.76 mL, 5.42 mmol, 1.4 eq.), and 100 mL of dry DCM. The flask was then placed in an ice bath on a magnetic stirrer and acryloyl chloride (0.38 mL, 4.64 mmol, 1.2 eq) was added dropwise. The reaction was left out at 0 °C for 2 h. The product was purified by extraction in DCM followed by column chromatography (hexane: ethyl acetate, 95:5) obtaining 0.98 g product with 81% yield. **^{1}H NMR (400 MHz, $CDCl_3$, δ, ppm):** 6.38 (d, 1H, H-J_1, J = 17.3 Hz) 6.11 (dd, 1H, H-I, J_1 = 10.4 Hz, J_2 = 17.3 Hz), 5.80 (d, 1H, H-J_2, J = 10.4 Hz), 4.13 (t, 4H, H-C), 3.44 (s, 2H, H-B), 2.23 (s, 3H, H-A), 1.64 (m, 4H, H–D), 1.28 (s, 12H, H-E). **^{13}C NMR (100 MHz, $CDCl_3$, δ, ppm):** 200.6 (C=O), 167.2 (C=O), 166.3 (C=O), 130.4 (CH_2), 128.6 (CH), 65.5 (CH_2), 64.7 (CH_2), 50.1 (CH_2), 30.1 (CH_3), 29.4 (CH_2), 29.2 (CH_2), 29.1 (CH_2), 28.6 (CH_2), 28.4 (CH_2), 25.9 (CH_2), 25.8 (CH_2). **FT-IR (ATR, ν) cm^{-1}:** 2936, 2855, 1718, 1636, 1466, 1408, 1359, 1295, 1270, 1239, 1187, 1150, 1057, 984, 810, 719, 669.

General procedure for RAFT polymerization of AcacP with cholX CholX and AcacP were dissolved in THF, and the mixture was degassed by bubbling it with argon for

15 min. AIBN was added after reaching 70 °C. The appropriate amounts of reagents are listed in Additional file 1: Table S1. After 24 h of polymerization, THF was evaporated on a rotary evaporator; then, the white residue was dissolved in DCM and precipitated in cold hexane. The product was filtered and dried in a oven (60 °C). **P2: ^{1}H NMR (400 MHz, $CDCl_3$, δ, ppm):** 4,12 (t, H–C from ketoester side, AcacP), 4.00 (s, H–C from polymer chain side, AcacP), 3.45 (s, H–B, AcacP), 2.27 (s, H–A, AcacP), 1.62 (m, H–D, AcacP), 1.29 (s, H–E, AcacP), 0.67 (s, 3H, chol-X). **FT-IR (ATR, ν) cm^{-1}:** 2925, 2854, 1728, 1460, 1359, 1238, 1158, 1047, 801, 719.

General procedure for RAFT block copolymerization of AcacP with chol-PNIPAAm-X Chol-PNIPAAm-X and AcacP were dissolved in THF, and the mixture was degassed by bubbling it with argon for 15 min. AIBN was added after reaching 70 °C. The appropriate amounts of reagents are listed in Additional file 1: Table S1. After 24 h of polymerization, THF was evaporated on a rotary evaporator; then, the white residue was dissolved in DCM and precipitated in cold hexane. The product was filtered and dried in a oven (60 °C). **P3: ^{1}H NMR (400 MHz, $CDCl_3$, δ, ppm):** 6.71 (NH, NIPAAm), 4.00 (C**H**$(CH_3)_2$, NIPAAm), 2.60–1.25 (polymer backbone), 1.15 (CH(C**H**$_3)_2$, NIPAAm). **FT–IR (ATR, ν) cm^{-1}:** 3293 (N–H), 3092, 3069, 2970, 2929, 2870, 1736, 1724, 1638 (C=O amide), 1535 (N–H), 1457, 1384, 1366, 1175, 1129, 976, 928, 878, 832.

General procedure for RAFT random copolymerization of NIPAAm and AcacP with cholX CholX, NIPAAm, and AcacP were dissolved in THF, and the mixture was degassed by bubbling it with argon for 15 min. AIBN was added after reaching 70 °C. The appropriate amounts of reagents are listed in Additional file 1: S1. After 24 h of polymerization, THF was evaporated on a rotary evaporator; then, the white residue was dissolved in DCM and precipitated in cold hexane. The product was filtered and dried in a oven (60 °C). **P4: ^{1}H NMR (400 MHz, $CDCl_3$, δ, ppm):** 6.60 (NH, NIPAAm), 4.00 (C**H**$(CH_3)_2$, NIPAAm), 2.40–1.25 (polymer backbone), 1.14 (CH(C**H$_3$**$)_2$, NIPAAm). **FT–IR (ATR, ν) cm^{-1}:** 3437 (N–H), 3292 (N–H), 3076, 2971, 2931, 2875, 1732, 1711, 1640 (C=O amide), 1537 (N–H), 1458, 1386, 1366, 1171, 1130, 976, 922, 884, 847.

General procedure for RAFT block copolymerization of NIPAAm with chol-PAcacP-X Chol-PAcacP-X and NIPAAm were dissolved in THF, and the mixture was degassed by bubbling with argon for 15 min. AIBN was added after reaching 70 °C. The appropriate amounts of reagents are listed in Additional file 1: Table S1. After 24 h of polymerization, THF was evaporated on a rotary evaporator; then, the white residue was dissolved in DCM and precipitated in cold hexane. The product was filtered and dried in a oven (60 °C). **P5: ^{1}H NMR (400 MHz, $CDCl_3$, δ, ppm):** 6.63 (NH, NIPAAm), 3.99 (CH$(CH_3)_2$, NIPAAm), 2.40–1.25 (polymer backbone), 1.14 (CH(C**H**$_3)_2$, NIPAAm). **FT–IR (ATR, ν) cm^{-1}:** 3286 (N–H), 3071, 2971, 2931, 2874, 1734, 1637 (C=O amide), 1536 (N–H), 1458, 1386, 1366, 1171, 1130, 974, 922, 884, 843.

Polymeric nanoparticles (PNPs) formation A 15 mg sample of a polymer was dissolved in 1.5 mL of THF and added dropwise to 15 mL of deionized water under vigorous stirring. It was then shaken for 24 h to achieve equilibrium. Next, the solution (16.5 mL) was dialyzed against water for 24 h. After dialysis, micelles were lyophilized. To facilitate the

description of the results, the polymers obtained by this method were marked with the prefix PN, for example, nanoparticles made from P1 were marked as PNP1.

Doxorubicin encapsulation during PNPs formation A 15 mg sample of a polymer was dissolved in a THF solution of DOX (1.5 mL, 0.58 mg mL^{-1}) and added dropwise to 15 mL of deionized water under vigorous stirring. It was then shaken for 24 h to achieve equilibrium. Next, the solution (16.5 mL) was dialyzed against water for 24 h. After dialysis, micelles were lyophilized. To facilitate the description of the results, the DOX-loaded polymeric nanoparticles obtained by this method were marked with the suffix DOX.

Doxorubicin release from polymeric nanoparticles A 5 mg sample of DOX-loaded micelles was dissolved in PBS (5 mL) and was sealed in a dialysis bag (Mw cutoff: 3500, Spectra/por). The dialysis bag was then incubated in PBS (100 mL) at 37 °C and 10 mL of incubation medium was taken at specified intervals. During this process, the volume was replenished with fresh PBS to the initial value. The released DOX content was determined based on fluorescence emission intensity analysis.

Results and discussion

Synthesis and characterization of polymers

Cholesterol-terminated poly(*N*-isopropylacrylamide) (**P1**) was synthesized following the previously described procedure (Misiak et al. 2020b). The monomer containing the ketoester group (**AcacP**) was obtained in two steps. In the first step, methyl acetoacetate was transesterified with 1,10-decanediol. In the second step, the reaction product was treated with acryloyl chloride. The **AcacP** was used to obtain the homopolymer (**P2**) by RAFT polymerization mediated by a cholesterol-functionalized dithiocarbonate. The block copolymers with different orders of blocks, **P3** and **P5**, were synthesized by the copolymerization of **P1** with **AcacP** and **P2** with NIPAAm, respectively. Additionally, a statistical copolymerization was performed to obtain a **P4** copolymer. Finally, five polymers with different structures and order of polymer blocks were obtained (Fig. 1).

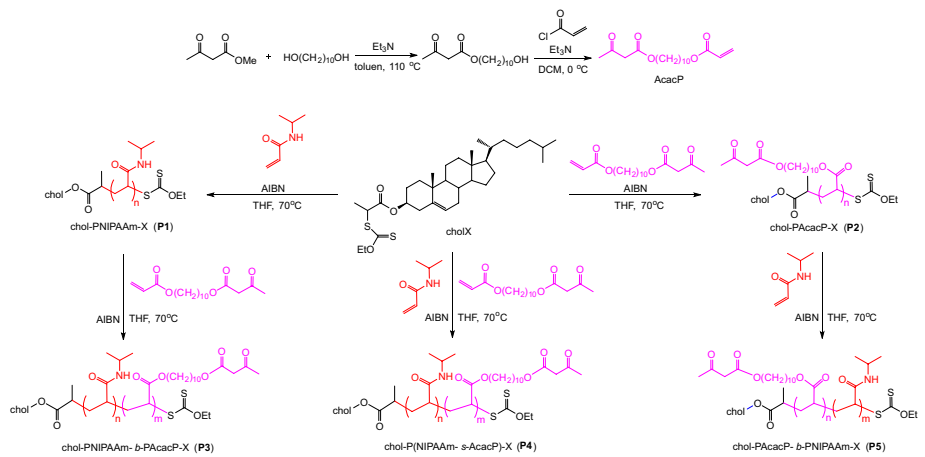

Fig. 1 Synthesis path of **AcacP**—monomer; **P3**—block copolymer with a keto-ester group at the end; **P4**—statistical copolymer; **P5**—block copolymer with PAcacP next to the cholesteryl moiety

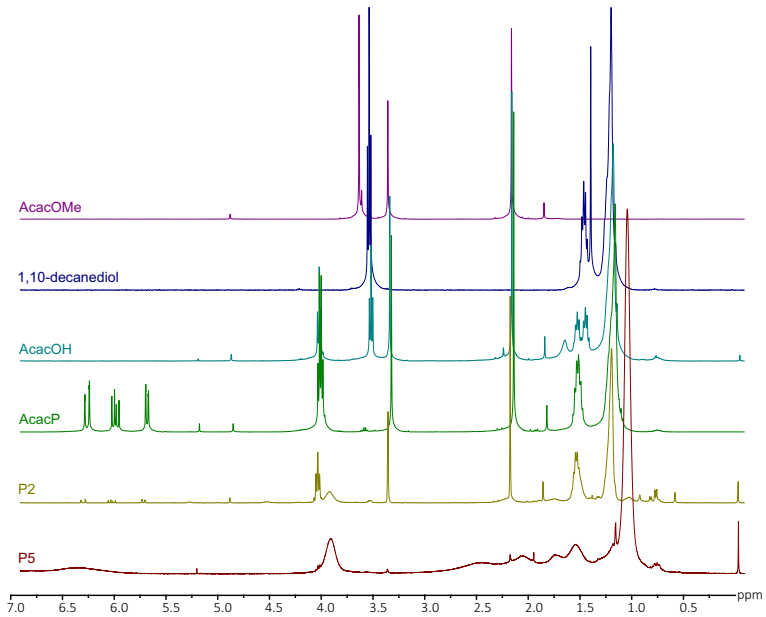

Fig. 2 Stacked ^{1}H NMR spectra along the synthetic path

Figure 2 shows stacked ^{1}H NMR spectra of starting materials and products along the synthetic path. The synthesis of a monosubstituted product was confirmed by the the appearance of a signal at 4.13 ppm and the remaining presence of a signal at 3.63 ppm, followed by matching the integration of the signals to the number of protons in the respective groups in the compound. Additionally, full spectra of **AcacOH** are presented in the supplementary information: ^{1}H NMR (Additional file 1: Fig. S1), ^{13}C NMR (Additional file 1: Fig. S2), DEPT (Additional file 1: Fig. S3), and FTIR (Additional file 1: Fig. S11). The synthesis of the ketoester monomer proceeded with an 81% yield. The presence of the **AcacP** is evidenced by the appearance of signals from the vinyl group in the range of 5.80–6.40 ppm and by a transition in the chemical shift of the CH_2 group next to the hydroxyl group, whose signal had disappeared. The full spectra of **AcacP** are shown in SI: ^{1}H NMR (Additional file 1: Fig. S4), ^{13}C NMR (Additional file 1: Fig. S5), DEPT (Additional file 1: Fig. S6), and FTIR (Additional file 1: Fig. S12). Subsequently, the disappearance of the signals from the vinyl group, the emergence of a new broad signal at 4.00 ppm from the polymer hydrocarbon backbone, and the appearance of a signal at 0.67 from **cholX** confirm that the homopolymer was obtained (**P2**). In the spectrum of the block copolymer (**P5**), signals from PNIPAAm are primarily visible, but low-intensity signals from **P2** are also present, e.g., at 3.40 or 2.27. RAFT polymerizations gave the desired homopolymers or copolymers with a conversion of at least 90%. The respective amounts of chemicals used are shown in Table 1 and the supporting information (Additional file 1: Table S1). All RAFT polymerizations were carried out for 24 h at 70 °C and the polymers were characterized by ^{1}H NMR (Additional file 1: Figs. S7–S10), and FTIR (Additional file 1: Figs. S13–S16).

The number-average molecular weights (M_n) of the polymers were calculated from SEC analysis or, in the case of **P2**, from the ^{1}H NMR spectrum (Additional file 1: Fig. S7). The values are shown in Table 1 and Additional file 1: Fig. S17. The molecular weights

Table 1 Synthetic details and results were obtained from NMR, SEC, and CMC measurements

Polymer	Conv[a] [%]	M_n[b] [kg mol^{-1}]	Đ[b]	CMC [mg mL^{-1}]
chol-PNIPAAm-X (**P1**)	99	26.42	1.10	0.0330
chol-PAcacP-X (**P2**)	95	5.65[c]	–	–
chol-PNIPAAm-*b*-PAcacP-X (**P3**)	> 99	29.47	1.07	0.0048
chol-P(NIPAAm-*s*-AcacP)-X (**P4**)	> 99	32.09	1.04	0.0110
chol-PAcacP-*b*-PNIPAAm-X (**P5**)	90	26.64	1.30	0.0050

[a] Monomer conversion determined by ^{1}H NMR

[b] Measured by SEC-RI-MALS

[c] Calculated from ^{1}H NMR. All polymerizations were carried out at 70 °C for 24 h, and AIBN was added as 10 mol% of CTA

of the **P1** and **P2** homopolymers are 26.42 kg mol^{-1} and 5.65 kg mol^{-1}, respectively. In the case of **P3** and **P5** block copolymers, an increase in M_n was observed. A statistical copolymer exhibits the highest molecular weight and the lowest dispersion. This may be related to the stiffening of the polymer chain caused by the presence of monomeric units in random order, which results in greater availability of the dithiocarbonate group. In turn, **P5** demonstrates the highest dispersion, which may be associated with a lower conversion (90%) compared to other polymers. It is impossible to clearly define the ratio of NIPAAm and AcacP units in polymers, however, the data indicate a similar proportion.

CMC determination

The obtained copolymers consist of blocks with different polarities, meaning they are capable of self-organizing into spatial systems. This phenomenon occurs when the critical micelle concentration (CMC) is exceeded. During the formation of polymer nanoparticles, it is also possible to encapsulate active substances. The spectrofluorimetric method of pyrene and linear regression (Additional file 1: Fig. S22) were used to determine the critical micelle concentrations.

Representative CMC measurement data: fluorescence emission spectra of pyrene with various concentrations of **P5** are presented in Additional file 1: Fig. S21. The CMCs of **P3**, **P4**, and **P5** were 0.0048, 0.0110, and 0.0050 mg mL^{-1}, respectively. The CMC values for the block copolymers are two times lower than the random copolymer, which may result from the order of the monomeric units in the polymer structure and the pronounced division into the hydrophilic and hydrophobic sides. **P1** represents the highest CMC value at 6 times higher than the block copolymers, which is directly related to its structure, which consists of a long part of the hydrophilic PNIPAAm and only one cholesteryl molecule at the end of the chain.

All further studies of empty and loaded PNPs were performed above the designated CMCs.

Nanoprecipitation of polymers into spatial systems with different physicochemical properties. Effect of doxorubicin encapsulation on the PNPs characteristics

Chemical or physical binding of DOX to a polymeric carrier offers many advantages: reduced toxicity compared to DOX in free form, more synchronized and controlled

pharmacokinetics, increased solubility and bioavailability, and the ability to bypass multi-drug resistance mechanisms (Lv et al. 2013; Mussi et al. 2014; Tahover et al. 2015).

Together, block copolymers and a random copolymer, with the unspecified alignment of molecules in the chain, will lead to obtaining polymer nanoparticles with a different arrangement of the unimers in the spatial structure. This may translate into PNPs of different sizes and result in changes in their physical and biological properties. It will also affect the encapsulation of doxorubicin, which will have a crucial effect in determining the structure–activity relationship (SAR).

Thermal analysis

The TG and DTG curves of empty and DOX-loaded PNPs are presented in Additional file 1: Fig. S19. A slight weight loss (< 5%) observed on the TG curves of all samples in the temperature range up to 100 °C is due to the removal of absorbed moisture. All the samples decompose quantitatively in one step between 350 and 450 °C, which is related to the depolymerization process. Generally, the degradation temperature decreases, and the maximum of the degradation rate shifts to lower T values when drug molecules are present. The glass transition (T_g) temperature of the empty and DOX-loaded PNPs was determined by DSC (Table 2, Additional file 1: Fig. S18). The T_g values for PNP1, PNP3, and PNP4 are close to 132 °C but it is much higher for PNP5 (138 °C). This is most likely related to a longer PAcacP block in the latter case. In general, the presence of doxorubicin does not affect the glass transition temperature values of (co)polymers. The exception is the PNP1_DOX, which contains much more doxorubicin than the other samples.

Cloud point and aggregation temperature measurements

The cloud point and aggregation temperature were determined using turbidimetry and DLS measurements in a change of temperature, respectively. The phase transition caused by temperature results in a shift of the equilibrium of polymer–solvent interactions toward intra- and intermolecular polymer–polymer interactions. This leads to aggregation of polymer chains and, as a result, turbidity of the solution (Kurowska et al. 2022a; b).

Aggregation of polymer blocks occurs around 30 °C, with the lowest temperature for the tested systems, 29 °C, determined for the random copolymer. The T_{agg} starts

Table 2 Physicochemical parameters of empty and doxorubicin-loaded nanoparticles

Polymer	MADLS [nm]	Horizontal size [nm]	Vertical size [nm]	Zeta potential [mV]	T_g [°C]	T_{CP} [°C]	T_{agg} [°C]	C_{DOX}[a] [μM]
PNP1	21.8 ± 3.0	17.7	13.6	− 6.8	132.5	34.0	30.5	
PNP1_DOX	24.1 ± 1.7	25.7	10.2	− 8.0	140.7	35.0	31.0	0.626
PNP3	99.7 ± 12.9	78.7	75.5	− 5.5	132.5	34.0	30.5	
PNP3_DOX	42.6 ± 2.8	29.1	28.1	− 24.2	132.2	33.5	30.5	0.163
PNP4	81.9 ± 5.0	59.0	18.5	− 3.7	131.8	30.5	29.0	
PNP4_DOX	86.4 ± 3.8	57.3	64.5	− 6.7	132.4	30.5	28.5	0.077
PNP5	30.1 ± 1.6	67.0	93.5	− 4.9	138.3	32.5	30.0	
PNP5_DOX	41.6 ± 1.3	32.4	28.6	− 7.9	139.8	33.0	30.0	0.190

[a] Determined in PBS solution of polymers at C = 1 mg mL^{-1}

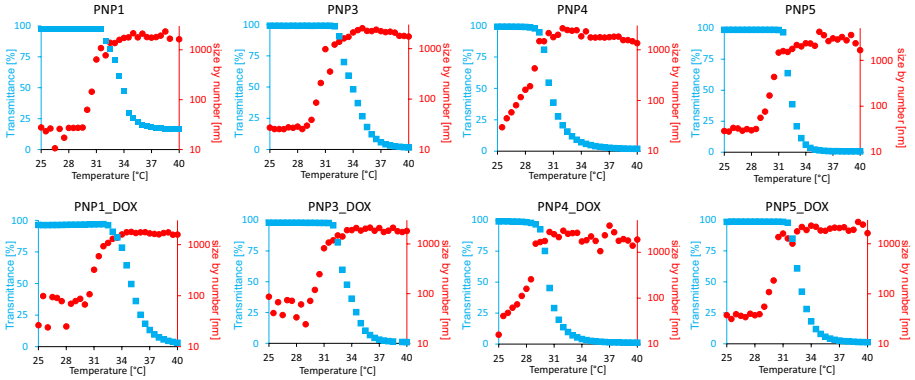

Fig. 3 Cloud point and aggregation temperatures of empty and DOX-loaded polymeric nanoparticles

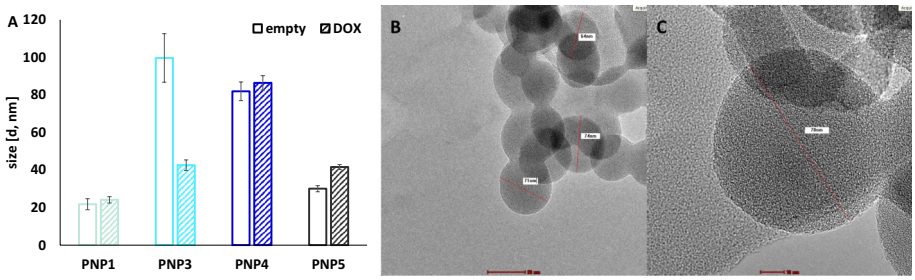

Fig. 4 Polymeric nanoparticles size **A** MADLS data in PBS at $C = 0.5$ mg mL^{-1} for empty and DOX-loaded PNPs, **B** and **C** TEM images with different magnifications of empty PNP3

3.5 °C earlier than the T_{CP} for PNP1 and PNP3, 1.5 °C earlier for PNP4, and 2.5 °C earlier for PNP5. The effect of doxorubicin on the aggregation temperature is negligible or unnoticed. The cloud point was determined as the temperature at which there is a rapid decrease in the transmission of the light beam by the sample and is shown in both Table 2 and Fig. 3. There is no significant effect on the T_{CP} of a ketoester block build-up (PNP3) compared to chol-PNIPAAm-X (PNP1). On the other hand, changing the structure of the polymer to a statistical (PNP4) or changing the order of the blocks (PNP5) leads to a decrease in the cloud point by 3.5 and 1.5 °C, respectively. Interestingly, reversing the order of blocks leads to a significant difference in T_{CP}. Doxorubicin encapsulation into copolymers PNP3, PNP4, and PNP5 does not significantly affect the cloud point. However, in the case of the PNP1 system, it leads to an increase of T_{CP} by 1° (Fig. 4).

Analysis of size, shape, and zeta potential (ZP) of polymeric nanoparticles

Size, shape, and zeta potential are key parameters determining the biodistribution and circulation time of drug delivery systems in vivo. The size of PNPs affects the pharmacokinetics, and adsorption of plasma proteins or affects the uptake at specific sites of cells. The polymer particles that will be used as carriers should have a size in the range of 20–150 nm. This reduces hepatic clearance and renal filtration mechanisms and prolongs the in vivo circulation time. Particles below 20 nm will be quickly excreted by the kidneys, while large particles will be easily picked up by the immune system (Di et al.

2021; Jasinski et al. 2018; Kim et al. 2011) Another important aspect is overcoming physiological barriers such as blood–brain, blood–gas, blood–retinal, blood–placental, and blood–pancreas (Di et al. 2021; Nowak et al. 2020). The addition of a block with a ketoester group to chol-PNIPAAm-X resulted in an almost fivefold increase in the particle size of the polymer nanoparticles from 21.8 for PNP1 to 99.7 for PNP3. This may be related to a different organization of unimers. For example, in the case of P1, we have a linear arrangement: hydrophobic cholesterol and hydrophilic PNIPAAm chain. In the case of block copolymers, the dissimilarity in particle size is interesting. PNP3 is more than 3 times larger than PNP5. However, after the introduction of doxorubicin, these sizes become equal. It, therefore, follows that the polymer chains interact in a specific way with DOX molecules, which forces a certain arrangement in space and an appropriate packing density in the polymer nanoparticle. In the case of a random copolymer, doxorubicin encapsulation does not change the hydrodynamic diameter of the particles. The results obtained using the dynamic light scattering technique are consistent with the particle sizes determined from TEM images, some of which are shown in Fig. 4B, C. The slight differences in size are due to the conditions of the measurement method (DLS—solution, TEM—sample evaporated on the grid). The size of the studied polymers, specifically in the range between 20 and 150 nm, is significant when the use of these polymers is studied in the future. It is crucial to prolong the circulation time in vivo and to avoid rapid excretion from the body.

As for the shape of the carriers, it will influence the macrophage clearance mechanisms, which will, in turn, lead to a change in the in vivo circulation time (Di et al. 2021; Gratton et al. 2008). It has been proven that spherical systems are characterized by the highest bioaccumulation in the clearance organs. In addition, spherical objects have the highest phagocytic potential of the known polymeric drug carrier shapes and are associated with the highest absorption rate by cells (Di et al. 2021). The Zetasizer Ultra has horizontal and vertical polarizing filters. Performing measurements using one filter or the other gives information about the shape of the analyzed particles. If the values in the vertical and horizontal directions coincide, it means that we are dealing with spherical objects. In the case of PNP3, PNP3_DOX, PNP4_DOX, and PNP5_DOX, the values of the hydrodynamic diameters obtained from measurements with polarizing filters are similar (Table 2). In addition, the spherical shape was confirmed by transmission electron microscopy imaging, which allows us to state that the doxorubicin-loaded polymer nanoparticles formed by the nanoprecipitation have the shape of a sphere, *i.e.,* the most desirable shape for use in drug delivery systems.

The surface charge will also be of great importance. Positively charged particles tend to interact with blood components, which may lead to hemolysis and toxic side effects on normal cells. On the other hand, negatively charged particles prolong the circulation time in vivo. However, strongly negative particles will reduce the internalization potential of the targeted cells (Di et al. 2021; Han et al. 2015; Roser et al. 1998). All tested PNP_DOX possess a correspondingly negative zeta potential to be used as drug delivery carriers. The increase in the absolute value of ZP after encapsulation of doxorubicin occurred in all nanoparticles. This allows the conclusion that DOX interacts with polymeric chains and improves the stability of the studied nanoparticles. The values obtained

from ELS measurements are listed in Table 2 and range between − 6.8 and − 3.7 for empty particles and − 6.7 to − 24.2 for loaded particles.

Determination of DOX in polymeric nanoparticles

The concentration of doxorubicin encapsulated in polymer nanoparticles was determined using the spectrofluorimetric method. The amounts of DOX were calculated from the equation of the standard curve shown in Additional file 1: Fig. S20. In the PNP3_DOX, PNP4_DOX and PNP5_DOX buffer solutions with a concentration of 1 mg mL^{-1}, the DOX concentrations were 0.163, 0.077 and 0.190 μM, respectively. The dose was found to be 4 –10 times lower than in the previously tested systems containing acetylacetone derivatives while maintaining efficacy against MCF-7 estrogen-dependent breast cancer cells (Misiak et al. 2022). The biologically tested PNPs' solution were appropriately diluted, which meant that the concentration of DOX in the vehicles was below the lowest dose currently used (0.5 μM). Unfortunately, it was impossible to determine the DOX release profile over time due to the small amounts used.

Biological studies

Evaluation of the hemocompatibility of drug carriers dedicated for intravenous injection is a key step to ensure good compatibility with the circulatory system. Since there is no standard preclinical in vivo examination method to perform a complex evaluation of the hemolytic reaction of a therapeutic agent, a hemocompatibility test using a hemolysis assay should be considered in toxicity studies of drug carriers (2021). It should also be emphasized that hemolytic reaction—hemolytic anemia (HA)—is the most common hematological problem that antineoplastic agents might induce in treated patients. It has been proven that the occurrence of anemia during anticancer treatment is > 53% and is higher in patients who received chemotherapy than in those who received concomitant chemo-radiotherapy (~ 42%) or radiotherapy alone (~ 20%) (Ludwig et al. 2004). Moreover, many reports indicated that nano-based preparations could also interact with the RBC membrane and lead to denaturation and impaired membrane functioning, which further contributes to its destruction (de la Harpe et al. 2019). In effect, hemolysis evaluation is widely used in the examination of different types of drug delivery systems. Figure 5A shows the results of the hemolysis assay after incubation of human RBC cells with synthesized polymeric nanoparticles—both empty and DOX-loaded applied within a concentration range from 0.05 up to 0.5 mg mL^{-1}. In all tested conditions, hemolysis ratios of all the samples are below the international standard level of 5% proposed for blood-contacting materials (Totea et al. 2014). However, the pharmaceutical guideline assumes that hemolysis between 10 and 25% is generally noted to be within relative limits (< 10% is considered non-hemolytic, and > 25% is considered hemolytic) (Amin and Dannenfelser 2006). Indeed, based on the obtained results synthesized PNPs have been confirmed to have good blood compatibility, and will be suitable as DOX carriers for intravenous administration. The aforementioned results are in agreement with our previously published studies, where compatibility with representatives of host cells has been confirmed (Misiak et al. 2020b, 2022). Further support for the current study is presented in results published by Xu et al. who reported a lack of hemolytic activity

after incubation of RBC cells with amphiphilic pH-sensitive nanoparticles based on imidazole/cholesterol modified hydroxyethyl starch (Xu et al. 2022).

It has been shown that, despite the benefits of systemic chemotherapy in breast cancer treatment, a percentage of patients with early-stage breast cancer will develop metastatic breast cancer (MBC). Anthracycline antibiotics, including doxorubicin, are recommended agents against MBC. However, the use of doxorubicin is linked to some life-threatening side effects including myelosuppression, disorder of the immune system, and cardiotoxicity. Many efforts have been made to lessen the negative side effects of doxorubicin and improve its efficacy (Ansari et al. 2017). To investigate the potential of synthesized polymers with cholesteryl moiety as drug carriers dedicated to DOX delivery, representatives of immune cells (Fig. 5B, C) and cardiomyocyte cells (Fig. 5D, E) were treated with different doses of the studied materials and DOX in free form. Evaluating the cytotoxic effect on monocytic THP-1 cells by measuring their ability to proliferate and their metabolic activity after treatment by synthesized PNPs is a crucial step during the assessment of anthracycline drug carriers' candidates. Therefore, the impact of the empty and DOX-loaded PNPs in comparison to DOX in free form was studied at a concentration of 0.5 μM, which corresponds to the concentration of DOX at carriers. The results presented in Fig. 5B indicate that treated cells are metabolically active in the presence of the tested agents. Notably, the addition of DOX in free form at a concentration of 0.5 μM causes a significant reduction of ~ 30% in THP-1 cell viability when compared to untreated cells. Meanwhile, DOX-loaded PNPs showed a statistically significant increased compatibility than DOX in free form. The greatest metabolic activity was indicated after the treatment of cells by copolymers applied at the highest concentration used. Interestingly, some increase in metabolic activity was observed in the case of DOX-loaded

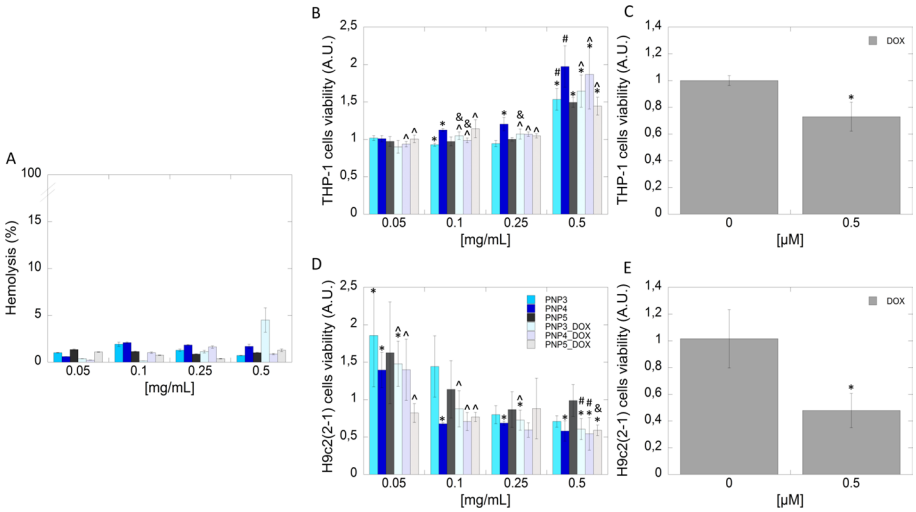

Fig. 5 Biocompatibility of the empty and DOX-loaded polymeric nanoparticles against representatives for normal cells. Hemolytic activity (**A**) and cell viability study on monocytic cells and cardiomyocyte cells after addition of bare and DOX-loaded polymeric nanoparticles (**B** and **D**) and DOX in free form (**C** and **E**). Statistical significance for the polymeric nanoparticles without or with DOX or DOX at free form vs. control was marked with (*); comparison of DOX (0.5 μM) at free vs encapsulated form PNP-DOX marked with (^) comparison of PNP vs PNP-DOX marked with ($^{\&}$), concentrations dependent response for PNP-DOX marked with ($^{\#}$), $p \leq 0.05$. The data presented constitute average results from three measurements ± SD

PNP3 and PNP4 in comparison to empty PNPs when added at concentrations 0.1 and 0.25 mg mL^{-1}. The tested materials generally presented low cytotoxicity in the case of cardiomyocyte cells. A statistically significant decrease in viability (~ 60%) was only observed for the highest dose of PNPs when compared to untreated control (Fig. 5D). Using the classification of cytotoxicity from ISO 10993-5, they could be ascribed to the third level of cytotoxicity — 80% — 60% viability, which means a weak cytotoxic effect (López-García et al. 2014). Moreover, a statistical analysis found that most PNPs-DOX showed better compatibility when compared to doxorubicin applied in free form. In turn, in the case of the incubation of cardiomyocyte cells with DOX in free form (0.5 μM), a marked decrease in cell viability—below 50% (moderate-strong cytotoxicity) was observed.

Figure 6A indicates a strong cytotoxic effect with viability below 40% of MCF-7 cells after treatment with a dose of PNP5_DOX. From a concentration of 0.1 mg mL^{-1} in the case of drug-loaded nanoparticles, a statistically significant decrease of MCF-7 cells viability, in a dose-dependent manner has been noted as compared to the control. A similar tendency has been indicated in the case of bare PNP, especially for PNP4 and PNP5 carriers. The application of all PNPs at the highest concentration caused a dramatic depletion of viable cells up to 5%, which is 16 times more than DOX in free form and 4-times more than estrogen-independent breast cancer cells.

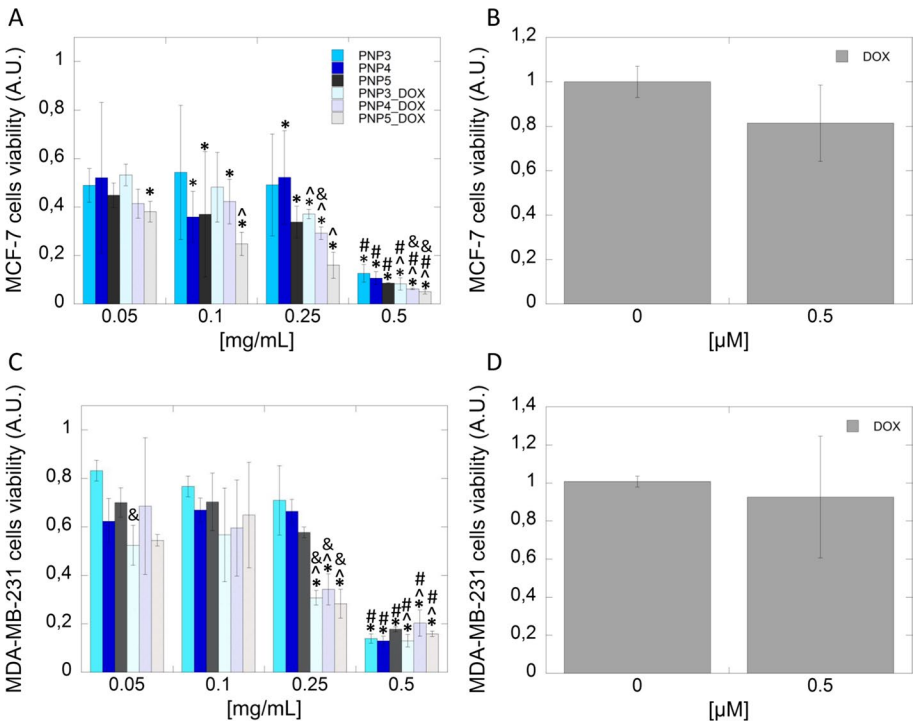

Fig. 6 Cytotoxic effect of the empty and DOX-loaded polymeric nanoparticles against estrogen-dependent and estrogen-independent breast cancer cells. Viability of estrogen-dependent (**A**) and estrogen-independent (**C**) breast cancer cells in the presence of empty and DOX-loaded polymeric nanoparticles containing DOX as well as free DOX (**B** and **D**). Statistical significance for the polymeric nanoparticles without or with DOX or DOX in free form vs. control was marked with (*); comparison of DOX (0.5 μM) at free vs encapsulated form PNP-DOX marked with ($^{\wedge}$) comparison of PNP vs PNP-DOX marked with ($^{\&}$), concentrations dependent response for PNP-DOX marked with ($^{\#}$), $p \leq 0.05$. The data presented constitute average results from three measurements ± SD

As shown in Fig. 6C, the negligible cytotoxic effect of bare PNPs at concentration range 0.05 to 0.25 as well as of DOX-loaded PNPs at concentration 0.05–0.1 mg mL^{-1} was indicated for estrogen-independent breast cancer cells. The increase in the DOX-loaded PNPs' concentration to 0.25 mg mL^{-1} caused a notable depletion of MDA-MB-231 cell viability when compared to untreated cells as well as those treated by free DOX and bare PNPs. In turn, at the highest concentration, both tested polymeric nanoparticles (bare and DOX-loaded) caused a statistically significant decrease in the percentage of viable cells. The mean viability was around 20%.

Since better efficacy was observed in the case of estrogen-dependent MCF-7 cells, the evaluation of the mode of action was performed on this kind of cell. To study the relative mechanism of synthesized polymeric nanocarriers cell cycle analysis, LDH-release assay, and ROS-generation assay were performed. The cell cycle is closely related to cell proliferation and cytotoxicity. In Fig. 7A–H profiles representing flow cytometry that present the cell cycle distribution with percentages of the cell population at each phase of the cell cycle are demonstrated. As can be seen in Fig. 7B, G2/M, S, and G0/G1 of cells exposed to DOX in free form with a concentration of 0.5 μM were normal and were not changed as compared to the control. The addition of empty as well as DOX-loaded PNPs might interfere with the cell cycle. In the case of pure block copolymers PNP3 and PNP5, a decrease in the percentage of cells up to 10.6 and 11.05%, respectively, in the S phase

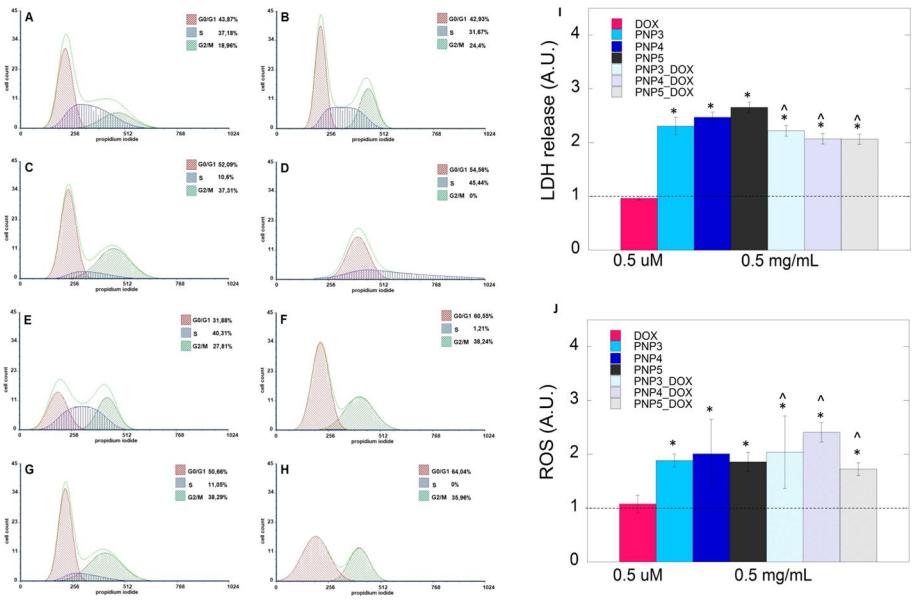

Fig. 7 The mode of action of empty and DOX-loaded polymeric nanoparticles against estrogen depends on breast cancer cells. The effect of tested compounds on cell cycle distribution in human breast cancer MCF-7 cell line is presented. Unstimulated cells (**A**) and cells exposed to DOX 0.5 μM (**B**), PNP3 (**C**), PNP3_DOX (**D**), PNP4 (**E**), PNP4_DOX (**F**), PNP5 (**G**), PNP5_DOX (**H**) were analyzed by DNA flow cytometry. LDH release from estrogen-dependent breast cancer cells (**I**) in the presence of the empty and DOX-loaded polymeric nanoparticles at the concentration of 0.5 mg mL^{-1} in comparison to free DOX 0.5 μM, Generation of reactive oxygen species (ROS) after treatment by bare and DOX-loaded polymeric nanoparticles at the concentration of 0.5 mg mL^{-1} in comparison to free DOX 0.5 μM (**J**). Statistical significance for the polymeric nanoparticles without or with DOX or DOX in free form *vs* control was marked with (*); comparison of DOX (0.5 μM) in free *vs* encapsulated form PNP-DOX marked with (^) $p \leq 0.05$. The data presented constitute average results from three measurements ± SD

was observed. In the case of PNP3_DOX, the total vanishing of the cells in the G2/M phase after loading DOX was noted. In turn, after treatment by DOX-loaded PNP4 and PNP5, the complete lack of cells in the S phase was detected. Due to the aforementioned results, it could be assumed that PNPs are internalized by cells and then distributed to the nucleus. This, in turn, could affect the DNA synthesis, and potentially induce apoptosis, thereby decreasing cell viability and proliferation. Based on the available literature, nanoparticles have been shown to cause cell cycle arrest, including G2/M, S, and G0/G1 phases (Ye et al. 2020). Undoubtedly, the type and extent of cell cycle arrest vary depending on the physicochemical characteristic including composition, size distribution, and surface modification (Li et al. 2018; Mahmoudi et al. 2011). It is generally accepted that G0/G1 arrest is associated with DNA damage and microtubule damage. However, a recent paper established that nanoparticles in combination with oxidative damage and/or lysosome rupture could lead to G0/G1 arrest (Li et al. 2018). Additionally, the paper published by Mahmoudi *et al.* suggested that the effects of nanoparticles on the cell cycle might mainly depend on the intracellular location of the nanoparticles. Ibiyeye *et al.* evaluated the effects of doxorubicin-loaded (Dox-ACNP), thymoquinone-loaded (TQ-ACNP), and a combined doxorubicin/thymoquinone-loaded cockle shell-derived aragonite calcium carbonate nanoparticles (Dox/TQ-ACNP) on a breast cancer cell line and compared the results with their free drugs counterparts on the cell cycle distribution (Ibiyeye et al. 2019). Results have shown that after treatment by Dox-ACNP, Dox/TQ, and Dox/TQ-ACNP the number of cells at the G2/M phase was increased at 72 h indicating cycle arrest. This effect might be related to their nuclear localization. However, the mechanisms and factors associated with the G2/M cell cycle arrest caused by nanoparticles are still unclear.

Our previously published results indicated that cholesterol might be used to modify drug carrier structure to improve cellular uptake of the drug-carrier conjugate (Markiewicz et al. 2021; Misiak et al. 2022). As shown in Fig. 7I, all tested carriers caused a 2–threefold increase in the LDH release from the treated cells. This confirms their ability to insert into the plasma membrane and is directly associated with the observed decrease in viability and disruption of the cell cycle. In agreement with the above, recently published studies have shown that modification of nanoparticles with hydrophobic moieties improves their adhesion to the plasma membrane through hydrophobic interactions (Wang et al. 2016; Zhang et al. 2019). Consequently, the aforementioned interactions enhanced nanoparticle uptake into cancer cells via lipid raft-dependent endocytosis (Niaz et al. 2022). The parallel hypothesis assumes that obtained PNPs might interact with the 17β-estradiol receptors which are overexpressed on the MCF-7 cells' surface (Misiak et al. 2022). This could explain higher cytotoxicity when ER-positive cells are treated. In effect, both nonspecific hydrophobic-based interaction and the receptor-dependent interaction could be considered.

It is established that the main source of increased cellular reactive oxygen species (ROS) levels is dysfunctional mitochondria. In effect, the altered oxidative status of the cell causes a specific vulnerability in cancer cells, which can be used as a therapeutic approach (Sullivan and Chandel 2014). One of the promising applications of nano-sized drug delivery systems in nanomedicine is transport to specific cellular targets, for example, mitochondria (Cho et al. 2020). The combination of treatment with exogenous ROS

generating agents, such as anthracycline antibiotics, along with the ability of NPs to impair the cellular antioxidant system might lead to exceeding a certain ROS threshold, resulting in detrimental oxidative damage (Brenneisen and Reichert 2018; Gurunathan et al. 2018). The above-mentioned oxidative stress cannot be equalized by the defense systems of cancer cells, inducing strong cytotoxic effects, disturbance of cell division, and lastly, cell death via apoptosis or necrosis (Sznarkowska et al. 2016). Our results indicated that treatment of MCF-7 cells by PNPs caused a twofold increase in ROS production when compared both to DOX in free form and to control cells. In turn, the use of DOX-loaded PNPs leads to an additional increment of ROS in treated cells. The abovementioned is supported by recently published studies (Li et al. 2021). For example, Leekha *et al.* observed a decrease in free radical scavengers including GSH, after treatment of MCF-7 cells by DOX-loaded chitosan nanoparticles (Leekha et al. 2019). Taken together, our results suggest that the observed cell cycle arrest and its associated DNA damage and cell death are partially triggered through ROS-mediated mechanism.

The use of nanocarriers as drug delivery systems (DDS) for targeted anticancer treatment has huge promise (Senapati et al. 2018). Among the advantages associated with the DDS application, one of the most important is the ability of carrier sensitization of cancer cells to low doses of therapeutic agents (Maroufi et al. 2020). The use of a chemotherapeutic agent at a low concentration reduces general toxicity and side effects and improves the patient's well-being and functioning (Rawat et al. 2021). In this study, the use of carriers with cholesterol moiety as a system for DOX delivery showed a great efficacy when compared to DOX in free form used at a similar concentration. In effect, our systems meet the aforementioned criteria dedicated to DDS that are needed to achieve better therapeutic efficacy as well as a significant reduction of the adverse impact of standard chemotherapy on patient quality of life. To date, several novel formulations of anthracyclines have been developed to improve compatibility via increasing the therapeutic index of anthracyclines (Leonard et al. 2009). For example, liposomal doxorubicin and pegylated liposomal doxorubicin showed favorable toxicity profiles with better cardiac safety and less myelosuppression, nausea, and vomiting, when compared to the anthracyclines in conventional form. The better therapeutic index of liposomal anthracyclines, achieved without compromising its efficacy makes it a beneficial choice over conventional anthracyclines in elderly patients, patients with high-risk factors for cardiac disease, and patients with prior use of anthracyclines (Green and Rose 2006; Rafiyath et al. 2012). Thus, based on our results, synthesized carriers might be promising candidates for preparing a novel formulation of anthracyclines. However, further in-deep pharmacokinetic and pharmacodynamics studies are needed to define the safety profile of proposed formulations.

Conclusion

The obtained polymer nanoparticles have a size, shape, and zeta potential suitable for drug delivery. The use of the copolymers shown may improve anthracycline-based chemotherapy. The results indicate that the proposed PNPs show good biocompatibility with blood and cause targeted cytotoxicity against estrogen-dependent breast cancer cells. The obtained doxorubicin vehicles led to the death of up to 90% of cancer cells. Disruption of the plasma membrane, ROS accumulation and cell cycle arrest are linked

to observed cellular deterioration, which consequently leads to cell death. It should be emphasized that the obtained nanosystems indicated better efficacy even though the DOX concentrations used in our studies are much lower than those described in the literature. This suggests that polymeric nanoparticles sensitize breast cancer cells to low doses of chemotherapeutic agents. Essentially, more in-depth studies involving animal models are required to select a great candidate for DOX delivery.

Abbreviations

AcacP	10-(Acryloyloxy)decyl-3-oxobutanoate
ACNP	Aragonite calcium carbonate nanoparticles
AIBN	2,2′-Azobis(2-methylpropionitrile)
ATR-FTIR	Attenuated total reflectance Fourier transform infrared spectroscopy
chol-X	O-ethyl-S-(1-cholesteroxycarbonyl)ethyldithiocarbonate
CMC	Critical micelle concentration
CTA	Chain transfer agent
DCM	Dichloromethane
DDS	Drug delivery systems
DEPT	Distortionless enhancement by polarization transfer
DLS	Dynamic light scattering
DMEM	Dulbecco's modified eagle medium
DNA	Deoxyribonucleic acid
DOX	Doxorubicin
DSC	Differential scanning calorimetry
ELS	Electrophoretic light scattering
GSH	Glutathione
HA	Hemolytic anemia
IRB	Institutional review board
LCST	Lower critical solution temperature
LDH	Lactate dehydrogenase
LN_2	Liquid nitrogen
MADLS	Multiangle dynamic light scattering
MBC	Metastatic breast cancer
MCF-7	Estrogen-dependent breast cancer cells
MDA-MB-231	Estrogen-independent breast cancer cells
M_n	Number-average molecular weight
Mw	Molecular weight
NMR	Nuclear magnetic resonance
NIPAAm	*N*-Isopropylacrylamide
PAcaP	Poly(10-(acryloyloxy)decyl-3-oxobutanoate)
PBS	Phosphate buffer solution
PEG	Poly(ethylene glycol)
PNIPAAm	Poly(*N*-isopropylacrylamide)
PNPs	Polymeric nanoparticles
PTFE	Polytetrafluoroethylene
RAFT/MADIX	Reversible addition-fragmentation chain transfer/macromolecular design by interchange of xanthate
RBC	Red blood cells
ROS	Reactive oxygen species
SAR	Structure activity relationship
SEC	Size exclusion chromatography
T_{agg}	Aggregation temperature
T_{CP}	Cloud point temperature
TEM	Transmission electron microscopy
T_g	Glass transition temperature
TGA	Thermogravimetric analyses
THF	Tetrahydrofuran
THP-1 cells	Human monocytic cell line
TQ	Thymoquinone
UV	Ultra violet

Supplementary Information

The online version contains supplementary material available at https://doi.org/10.1186/s12645-023-00176-9.

Additional file 1. Additional figures and table.

Acknowledgements
Analyses were performed in the Centre of Synthesis and Analysis BioNanoTechno of the University of Bialystok. The equipment in the Centre was funded by the EU as a part of the Operational Program Development of Eastern Poland 2007-2013, projects: POPW.01.03.00-20-034/09-00 and POPW.01.03.00-20-004/11.

Author contributions
PM: investigation, writing—original draft, visualization, KNL: investigation, writing—original draft, visualization, conceptualization of biological part, KHM: investigation, writing—review and editing, PW, IK, RC: investigation, IMT: investigation, writing—review and editing, HC: writing—review and editing, KB: review, AZW: conceptualization, supervision, writing—review and editing, project administration, funding acquisition. All authors read and approved the final manuscript.

Funding
This work was financially supported by the National Science Centre, Poland, grant no. NCN/2016/21/B/ST5/01365.

Availability of data and materials
The results/data/figures in this manuscript have not been published elsewhere, nor are they under consideration (from you or one of your Contributing Authors) by another publisher. All of the material is owned by the authors and/or no permissions are required.

Declarations

Ethics approval and consent to participate
The hemolytic activity of the tested polymeric nanoparticles was evaluated in blood samples from healthy adult volunteers under IRB approval: R-I-002/245/2019. This study was approved by the Institutional Review Board (IRB) of The Medical University of Bialystok. All subjects provided informed written consent, and the collected samples were anonymous.

Consent for publication
All authors have approved the final version of the manuscript.

Competing interests
The authors declare that they have no competing interests.

Received: 30 June 2022 Accepted: 9 March 2023
Published online: 21 March 2023

References

Amin K, Dannenfelser R-M (2006) In vitro hemolysis: guidance for the pharmaceutical scientist. J Pharm Sci 95(6):1173–1176
Ansari L, Shiehzadeh F, Taherzadeh Z, Nikoofal-Sahlabadi S, Momtazi-borojeni AA, Sahebkar A et al (2017) The most prevalent side effects of pegylated liposomal doxorubicin monotherapy in women with metastatic breast cancer: a systematic review of clinical trials. Cancer Gene Ther 24(5):189–193
Avramović N, Mandić B, Savić-Radojević A, Simić T (2020) Polymeric nanocarriers of drug delivery systems in cancer therapy. Pharmaceutics 12(4):298
Bray F, Ferlay J, Soerjomataram I, Siegel RL, Torre LA, Jemal A (2018) Global cancer statistics 2018: GLOBOCAN estimates of incidence and mortality worldwide for 36 cancers in 185 countries. CA Cancer J Clin 68(6):394–424
Brenneisen P, Reichert AS (2018) Nanotherapy and reactive oxygen species (ROS) in cancer: a novel perspective. Antioxidants 7(2):31
Cammas S, Suzuki K, Sone C, Sakurai Y, Kataoka K, Okano T (1997) Thermo-responsive polymer nanoparticles with a core-shell micelle structure as site-specific drug carriers. J Control Release 48(2–3):157–164
Carvalho C, Santos XR, Cardoso S, Correia S, Oliveira JP, Santos SM et al (2009) Doxorubicin: the good, the bad and the ugly effect. Curr Med Chem 16(25):3267–3285
Cerqueira NMFSA, Oliveira EF, Gesto DS, Santos-Martins D, Moreira C, Moorthy HN et al (2016) Cholesterol biosynthesis: a mechanistic overview. Biochemistry 55(39):5483–5506
Chen H-H, Lu I-L, Liu T-I, Tsai Y-C, Chiang W-H, Lin S-C et al (2019) Indocyanine green/doxorubicin-encapsulated functionalized nanoparticles for effective combination therapy against human MDR breast cancer. Colloids Surf B Biointerfaces 177:294–305
Cho H, Cho Y-Y, Shim MS, Lee JY, Lee HS, Kang HC (2020) Mitochondria-targeted drug delivery in cancers. Biochim Biophys Acta BBA Mol Basis Dis. 1866(8):165808
d'Avanzo N, Torrieri G, Figueiredo P, Celia C, Paolino D, Correia A et al (2021) LinTT1 peptide-functionalized liposomes for targeted breast cancer therapy. Int J Pharm 597:120346
de la Harpe KM, Kondiah PPD, Choonara YE, Marimuthu T, du Toit LC, Pillay V (2019) The hemocompatibility of nanoparticles: a review of cell-nanoparticle interactions and hemostasis. Cells 8(10):1209
Di J, Gao X, Du Y, Zhang H, Gao J, Zheng A (2021) Size, shape, charge and "stealthy" surface: carrier properties affect the drug circulation time in vivo. Asian J Pharm Sci 16(4):444–458
Don T-M, Lu K-Y, Lin L-J, Hsu C-H, Wu J-Y, Mi F-L (2017) Temperature/pH/enzyme triple-responsive cationic protein/PAA-*b*-PNIPAAm nanogels for controlled anticancer drug and photosensitizer delivery against multidrug resistant breast cancer cells. Mol Pharm 14(12):4648–4660
Du M, Ouyang Y, Meng F, Ma Q, Liu H, Zhuang Y et al (2019) Nanotargeted agents: an emerging therapeutic strategy for breast cancer. Nanomed Future Med 14(13):1771–1786

Frederick CA, Williams LD, Ughetto G, Van der Marel GA, Van Boom JH, Rich A et al (1990) Structural comparison of anti-cancer drug-DNA complexes: adriamycin and daunomycin. Biochemistry 29(10):2538–2549
Gonçalves M, Mignani S, Rodrigues J, Tomás H (2020) A glance over doxorubicin based-nanotherapeutics: from proof-of-concept studies to solutions in the market. J Control Release 317:347–374
Gratton SEA, Ropp PA, Pohlhaus PD, Luft JC, Madden VJ, Napier ME et al (2008) The effect of particle design on cellular internalization pathways. Proc Natl Acad Sci 105(33):11613–11618
Green AE, Rose PG (2006) Pegylated liposomal doxorubicin in ovarian cancer. Int J Nanomedicine 1(3):229–239
Gurunathan S, Kang M-H, Qasim M, Kim J-H (2018) Nanoparticle-mediated combination therapy: two-in-one approach for cancer. Int J Mol Sci 19(10):3264
Han S-S, Li Z-Y, Zhu J-Y, Han K, Zeng Z-Y, Hong W et al (2015) Dual-pH sensitive charge-reversal polypeptide micelles for tumor-triggered targeting uptake and nuclear drug delivery. Small 11(21):2543–2554
He W, Ma Y, Gao X, Wang X, Dai X, Song J (2020) Application of poly(N-isopropylacrylamide) as thermosensitive smart materials. J Phys Conf Ser 1676:012063
Hortobágyi GN (1997) Anthrazykline in der Krebstherapie: Ein Überblick. Drugs 54(Supplement 4):1–7
Ibiyeye KM, Nordin N, Ajat M, Zuki ABZ (2019) Ultrastructural changes and antitumor effects of doxorubicin/thymoquinone-loaded $CaCO_3$ nanoparticles on breast cancer cell line. Front Oncol. https://doi.org/10.3389/fonc.2019.00599
Jasinski DL, Li H, Guo P (2018) The effect of size and shape of RNA nanoparticles on biodistribution. Mol Ther 26(3):784–792
Kim S, Oh W-K, Jeong YS, Hong J-Y, Cho B-R, Hahn J-S et al (2011) Cytotoxicity of, and innate immune response to, size-controlled polypyrrole nanoparticles in mammalian cells. Biomaterials 32(9):2342–2350
Kurowska I, Amouroux B, Langlais M, Coutelier O, Coudret C, Destarac M et al (2022a) Versatile thiolactone-based conjugation strategies to polymer stabilizers for multifunctional upconverting nanoparticles aqueous dispersions. Nanoscale. https://doi.org/10.1039/d1nr05548h
Kurowska I, Markiewicz KH, Niemirowicz-Laskowska K, Misiak P, Destarac M, Wielgat P et al (2022b) Membrane-active diacylglycerol-terminated thermoresponsive polymers: RAFT synthesis and biocompatibility evaluation. Eur Polym J 169:111154
Leekha A, Kumar V, Moin I, Gurjar BS, Verma AK (2019) Modulation of oxidative stress by doxorubicin loaded chitosan nanoparticles. J Cancer Res Pract 6(2):76
Leonard RCF, Williams S, Tulpule A, Levine AM, Oliveros S (2009) Improving the therapeutic index of anthracycline chemotherapy: Focus on liposomal doxorubicin (Myocet™). Breast 18(4):218–224
Li Q, Huang C, Liu L, Hu R, Qu J (2018) Effect of surface coating of gold nanoparticles on cytotoxicity and cell cycle progression. Nanomaterials 8(12):1063
Li Y, Yang J, Sun X (2021) Reactive oxygen species-based nanomaterials for cancer therapy. Front Chem. https://doi.org/10.3389/fchem.2021.650587
López-García J, Lehocký M, Humpolíček P, Sáha P (2014) HaCaT keratinocytes response on antimicrobial atelocollagen substrates: extent of cytotoxicity, cell viability and proliferation. J Funct Biomater 5(2):43–57
Ludwig H, Van Belle S, Barrett-Lee P, Birgegård G, Bokemeyer C, Gascón P et al (2004) The European Cancer Anaemia Survey (ECAS): a large, multinational, prospective survey defining the prevalence, incidence, and treatment of anaemia in cancer patients. Eur J Cancer 40(15):2293–2306
Lv S, Li M, Tang Z, Song W, Sun H, Liu H et al (2013) Doxorubicin-loaded amphiphilic polypeptide-based nanoparticles as an efficient drug delivery system for cancer therapy. Acta Biomater 9(12):9330–9342
Mahmoudi M, Azadmanesh K, Shokrgozar MA, Journeay WS, Laurent S (2011) Effect of nanoparticles on the cell life cycle. Chem Rev 111(5):3407–3432
Markiewicz KH, Niemirowicz-Laskowska K, Szymczuk D, Makarewicz K, Misztalewska-Turkowicz I, Wielgat P et al (2021) Magnetic particles with polymeric shells bearing cholesterol moieties sensitize breast cancer cells to low doses of doxorubicin. Int J Mol Sci 22(9):4898
Maroufi NF, Vahedian V, Mazrakhondi SAM, Kooti W, Khiavy HA, Bazzaz R et al (2020) Sensitization of MDA-MBA231 breast cancer cell to docetaxel by myricetin loaded into biocompatible lipid nanoparticles via sub-G1 cell cycle arrest mechanism. Naunyn Schmiedebergs Arch Pharmacol 393(1):1–11
Metawea ORM, Abdelmoneem MA, Haiba NS, Khalil HH, Teleb M, Elzoghby AO et al (2021) A novel 'smart' PNIPAM-based copolymer for breast cancer targeted therapy: synthesis, and characterization of dual pH/temperature-responsive lactoferrin-targeted PNIPAM-co-AA. Colloids Surf B Biointerfaces 202:111694. https://doi.org/10.1016/j.colsurfb.2021.111694
Misiak P, Markiewicz KH, Szymczuk D, Wilczewska AZ (2020a) Polymeric drug delivery systems bearing cholesterol moieties: a review. Polymers 12(11):2620
Misiak P, Niemirowicz-Laskowska K, Markiewicz KH, Misztalewska-Turkowicz I, Wielgat P, Kurowska I et al (2020b) Evaluation of cytotoxic effect of cholesterol end-capped poly(N-isopropylacrylamide)s on selected normal and neoplastic cells. Int J Nanomedicine 15:7263–7278
Misiak P, Niemirowicz-Laskowska K, Misztalewska-Turkowicz I, Markiewicz KH, Wielgat P, Car H et al (2022) Doxorubicin delivery systems with an acetylacetone-based block in cholesterol-terminated copolymers: diverse activity against estrogen-dependent and estrogen-independent breast cancer cells. Chem Phys Lipids 245:105194. https://doi.org/10.1016/j.chemphyslip.2022.105194
Mussi SV, Sawant R, Perche F, Oliveira MC, Azevedo RB, Ferreira LAM et al (2014) Novel nanostructured lipid carrier co-loaded with doxorubicin and docosahexaenoic acid demonstrates enhanced in vitro activity and overcomes drug resistance in MCF-7/Adr cells. Pharm Res 31(8):1882–1892
Nes WD (2011) Biosynthesis of cholesterol and other sterols. Chem Rev 111(10):6423–6451
Niaz S, Forbes B, Raimi-Abraham BT (2022) Exploiting endocytosis for non-spherical nanoparticle cellular uptake. Nanomanufacturing 2(1):1–16
Nowak M, Brown TD, Graham A, Helgeson ME, Mitragotri S (2020) Size, shape, and flexibility influence nanoparticle transport across brain endothelium under flow. Bioeng Transl Med. https://doi.org/10.1002/btm2.10153

Olim F, Neves AR, Vieira M, Tomás H, Sheng R (2021) Self-assembly of cholesterol-doxorubicin and TPGS into prodrug-based nanoparticles with enhanced cellular uptake and lysosome-dependent pathway in breast cancer cells. Eur J Lipid Sci Technol 123(5):2000337
Paul Launchbury A, Habboubi N (1993) Epirubicin and doxorubicin: a comparison of their characteristics, therapeutic activity and toxicity. Cancer Treat Rev 19(3):197–228
Pigram WJ, Fuller W, Hamilton LD (1972) Stereochemistry of intercalation: interaction of daunomycin with DNA. Nat New Biol 235(53):17–19
Pommier Y, Leo E, Zhang H, Marchand C (2010) DNA topoisomerases and their poisoning by anticancer and antibacterial drugs. Chem Biol 17(5):421–433
Rafiyath SM, Rasul M, Lee B, Wei G, Lamba G, Liu D (2012) Comparison of safety and toxicity of liposomal doxorubicin vs. conventional anthracyclines: a meta-analysis. Exp Hematol Oncol 1(1):10
Rawat PS, Jaiswal A, Khurana A, Bhatti JS, Navik U (2021) Doxorubicin-induced cardiotoxicity: an update on the molecular mechanism and novel therapeutic strategies for effective management. Biomed Pharmacother 139:111708
Rivankar S (2014) An overview of doxorubicin formulations in cancer therapy. J Cancer Res Ther 10(4):853
Roser M, Fischer D, Kissel T (1998) Surface-modified biodegradable albumin nano- and microspheres. II: effect of surface charges on in vitro phagocytosis and biodistribution in rats. Eur J Pharm Biopharm 46(3):255–263
Sadava DE (ed) (2011) Life: the science of biology, 9th edn. Sinauer Associates, W. H. Freeman & Co, Sunderland
Safra T (2003) Cardiac safety of liposomal anthracyclines. Oncologist 8(S2):17–24
Senapati S, Mahanta AK, Kumar S, Maiti P (2018) Controlled drug delivery vehicles for cancer treatment and their performance. Signal Transduct Target Ther 3(1):1–19
Shan K, Lincoff AM, Young JB (1996) Anthracycline-induced cardiotoxicity. Ann Intern Med 125(1):47–58
Shin HH, Choi HW, Lim JH, Kim JW, Chung BG (2020) Near-infrared light-triggered thermo-responsive poly(N-isopropylacrylamide)-pyrrole nanocomposites for chemo-photothermal cancer therapy. Nanoscale Res Lett 15(1):214. https://doi.org/10.1186/s11671-020-03444-4
Sullivan LB, Chandel NS (2014) Mitochondrial reactive oxygen species and cancer. Cancer Metab 2(1):17
Sung H, Ferlay J, Siegel RL, Laversanne M, Soerjomataram I, Jemal A et al (2021) Global cancer statistics 2020: GLOBOCAN estimates of incidence and mortality worldwide for 36 cancers in 185 countries. CA Cancer J Clin 71(3):209–249
Sznarkowska A, Kostecka A, Meller K, Bielawski KP (2016) Inhibition of cancer antioxidant defense by natural compounds. Oncotarget 8(9):15996–16016
Tacar O, Sriamornsak P, Dass CR (2012) Doxorubicin: an update on anticancer molecular action, toxicity and novel drug delivery systems. J Pharm Pharmacol 65(2):157–170
Tahover E, Patil YP, Gabizon AA (2015) Emerging delivery systems to reduce doxorubicin cardiotoxicity and improve therapeutic index: focus on liposomes. Anticancer Drugs 26(3):241–258
Thigpen JT (2005) Innovations in anthracycline therapy: overview. Commun Oncol 2:3–7
Torchilin VP (2012) Multifunctional nanocarriers. Adv Drug Deliv Rev 64:302–315
Totea G, Ionita D, Demetrescu I, Mitache M (2014) *In vitro* hemocompatibility and corrosion behavior of new Zr-binary alloys in whole human blood. Open Chem 12(796–803):796
Volkova M, Russell R (2012) Anthracycline cardiotoxicity: prevalence, pathogenesis and treatment. Curr Cardiol Rev 7(4):214–220
Wang H-Y, Hua X-W, Jia H-R, Liu P, Gu N, Chen Z et al (2016) Enhanced cell membrane enrichment and subsequent cellular internalization of quantum dots via cell surface engineering: illuminating plasma membranes with quantum dots. J Mater Chem B 4(5):834–843
Wang YM, Zheng SX, Chang HI, Tsai HY, Liang M (2017) Microwave-assisted synthesis of thermo- and pH-responsive antitumor drug carrier through reversible addition–fragmentation chain transfer polymerization. Express Polym Lett 11(4):293–307
Wang H, Li Z, Lu S, Li C, Zhao W, Zhao Y et al (2020) Nano micelles of cellulose-graft-poly (L-lactic acid) anchored with epithelial cell adhesion antibody for enhanced drug loading and anti-tumor effect. Mater Today Commun 22:100764
Wicki A, Witzigmann D, Balasubramanian V, Huwyler J (2015) Nanomedicine in cancer therapy: Challenges, opportunities, and clinical applications. J Controlled Release 200:138–157
Xu Z, Yang D, Long T, Yuan L, Qiu S, Li D et al (2022) pH-Sensitive nanoparticles based on amphiphilic imidazole/cholesterol modified hydroxyethyl starch for tumor chemotherapy. Carbohydr Polym 277:118827
Yang F, Teves SS, Kemp CJ, Henikoff S (2014) Doxorubicin, DNA torsion, and chromatin dynamics. Biochim Biophys Acta BBA Rev Cancer 1845(1):84–89
Yang C, Liu SQ, Venkataraman S, Gao SJ, Ke X, Chia XT et al (2015) Structure-directing star-shaped block copolymers: Supramolecular vesicles for the delivery of anticancer drugs. J Controlled Release 208:93–105
Ye P, Ye Y, Chen X, Zou H, Zhou Y, Zhao X et al (2020) Ultrasmall Fe_3O_4 nanoparticles induce S-phase arrest and inhibit cancer cells proliferation. Nanotechnol Rev 9(1):61–69
Zhang Y, Xiao C, Li M, Ding J, Yang C, Zhuang X et al (2014) Co-delivery of doxorubicin and paclitaxel with linear-dendritic block copolymer for enhanced anti-cancer efficacy. Sci China Chem 57(4):624–632
Zhang CY, Chen Q, Wu WS, Guo XD, Cai CZ, Zhang LJ (2016) Synthesis and evaluation of cholesterol-grafted PEGylated peptides with pH-triggered property as novel drug carriers for cancer chemotherapy. Colloids Surf B Biointerfaces 142:55–64
Zhang R, Qin X, Kong F, Chen P, Pan G (2019) Improving cellular uptake of therapeutic entities through interaction with components of cell membrane. Drug Deliv 26(1):328–342

Publisher's Note